Numerical developments of lateral pile-soil behavior in pile driving

Allani, M. & Holeyman, A.
Université Catholique de Louvain

Keywords: finite element, eccentric, pile driving, lateral soil reaction

ABSTRACT: The objective of this paper is to model the lateral pile/soil behavior due to eccentric impacts in pile driving. A 1-D finite element model representing the pile is coupled to a 2-D radial discretisation of the surrounding soil. The pile is considered in the model as an Euler-Bernoulli vertical beam. Radial and tangential discretisations of the soil medium are proposed to model the soil reaction based on equilibrium equations in cylindrical coordinates. Both pile and soil vibrations are coupled in the time domain by calculating the lateral soil reaction at each time step. After the validation of the model, recorded bending moments form in-situ real cases due to eccentric impacts are applied in the model to study the flexural pile and lateral soil vibration. Finally, comparison of simulation and measurement show the practical usefulness of the model.

1 INTRODUCTION

High strain dynamic pile testing aims at evaluating the pile bearing capacity. It is nowadays a routinely used technique and several methods exist to process the measured signals in the field for a better extraction of the soil resistance. The Case method (Rausche et al, 1985, 2000), NUSUMS (Holeyman, 1992) and CAPWAP (Rausche, 2000) are examples of programs dedicated to that purpose. The one-dimensional longitudinal wave equation coupled with Winkler soil reactions is the approach used in nearly all pile driving programs to model the pile axial behavior.

However, several authors signaled the occurrence of flexural pile vibrations in Dynamic Loading Tests (DLTs). Poskitt (1992), Holeyman (2000) and Charue (2004) indicated that eccentricity of the mass ram relative to the neutral pile axis and pile inclination are reasons for the flexural vibration of piles in DLTs. It is also well observed in pile driving where extreme conditions may be reached. Poskitt (1991, 1992 and 1996) used an equivalent Smith's (1960) soil reaction model to represent the lateral soil reaction. He used the Newtonian impact theory to model the eccentricity. No pile elasticity was taken into account and lateral soil reaction was treated by analogy to axial soil resistance (Winkler approach with Smith (1960) damping). No further developments have been encountered in the literature to properly model the lateral behavior under pile driving. The latter is much more complicated than the axial one. Furthermore, most of the developed solutions for lateral pile vibration are limited to harmonic loading (Novak and Nogami 1977, Nogami and Novak 1977, Novak et al 1978, Yao and Nogami 1994, El Naggar and Novak 1995, El Naggar and Novak 1996, Chau and Yang 2005).

Since pile driving is an essentially transient problem, it is necessary in the authors' opinion to create a specific model that can address the transient lateral behavior of both pile and soil during pile driving.

In this paper, a numerical program is presented to model the transient lateral pile-soil interaction during pile driving. Measured bending moment in filed due to the eccentricity is introduced in the numerical program to study the lateral pile and soil vibration.

A finite element program is first presented where pile bending is calculated using a vertical Euler-Bernoulli beam. Then we propose a continuum approach for the lateral soil reaction. The highly transient character of the test is easily incorporated in the pile and soil representation. The adopted approach is similar to that proposed by Holeyman (1984, 1994) for continuum modeling of axial shaft soil reaction. The pile finite element model is coupled in the time domain with the soil lateral reaction. Numerical solutions and in-situ measurements (Allani and Holeyman, 2012) of flexural pile behavior are finally compared.

2 PHYSICAL MODEL REPRESENTATION

In this section we state the problem and the different physical aspects incorporated in the numerical analysis. The proposed problem deals with a pile foundation modeled as a vertical Euler-Bernoulli column partially embedded in the soil medium. The pile is subjected to an eccentric impact provided by a mass via a pile cushion at the pile head (Fig 1.a).

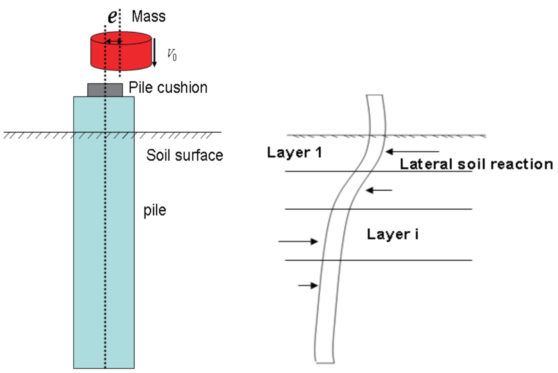

Figure 1. a) Eccentric pile driving b) Lateral pile movement and soil reaction.

In fact, lateral pile movement due to the eccentric impact induces a dynamic lateral soil reaction. The pile is divided into a number of equal length elements to match soil layers (Fig 1.b).

3 PILE FINITE ELEMENT FORMULATION

3.1 *Pile modeling: finite element formulation*

This section presents the formulation of the lateral pile behavior using Hamilton's principle. The pile elements possess two nodes *i* and *j*; each node has three degrees of freedom, i.e. axial displacement, lateral displacement and rotation (Fig. 2). We define v^e as the lateral displacement element and θ^e as the element rotation. Hermitian shape functions are used for the Euler-Bernoulli lateral pile vibration. However, for the axial finite element formulation, the conventional 1st polynomial order is used for the shape functions. Since in our case both axial and lateral vibrations are considered, pile element matrices have 6×6 size.

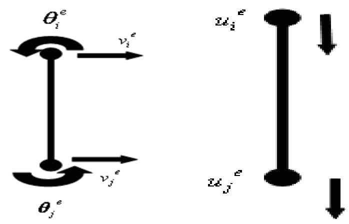

Figure 2. 2-node element for a) lateral pile displacement b) axial pile displacement.

The equation of pile motion in matrix form is writen as:

$$[M]\{\ddot{U}\}+[C]\{\dot{U}\}+[K]\{U\}=[F] \quad (1)$$

where $\{U\}$, $\{\dot{U}\}$ and $\{\ddot{U}\}$ are pile displacement, velocity and acceleration vectors while $[F]$, $[M]$, $[C]$ and $[K]$ are force, mass, damping and stiffness matrices respectively.

Step by step time integration is expressed in matrix form as:

$$\left(\frac{M}{\Delta t^2}+\frac{C}{2\Delta t}\right)U_{t+\Delta t}=F_t-\left(K-\frac{2M}{\Delta t^2}\right)U_t-\left(\frac{M}{\Delta t^2}-\frac{C}{2\Delta t}\right)U_{t-\Delta t} \quad (2)$$

where $U_{t+\Delta t}$, U_t and $U_{t-\Delta t}$ are displacement at the time $t+\Delta t$, t and $t-\Delta t$ respectively with Δt the time integration increment.

In order to maintain numerical stability, the time increment should be small enough so that information does not travel faster than the compressive wave propagation velocity c_p. This condition can be expressed, for a pile length element L_i, as:

$$\Delta t < \frac{L_i}{c_p} \quad (3)$$

where $c_p = \sqrt{E_p / \rho_p}$ is the bar velocity, E_p and ρ_p are the pile Young modulus and pile density.

The central difference explicit scheme is used to compute the pile vibration. The pile velocity and acceleration are expressed respectively as:

$$V_t = \frac{U_{t+\Delta t}+U_{t-\Delta t}}{2\Delta t} \quad (4)$$

and

$$A_t = \frac{U_{t+\Delta t}-2U_t+U_{t-\Delta t}}{\Delta t^2} \quad (5)$$

Although only the classical Euler-Bernoulli finite element formulation is presented in this paper for the lateral pile vibration, the program also incorporates the finite element formulation in accordance to the more extended Timoshenko beam theory. This formulation is presented in detail in Allani and Holeyman (2010) and was inspired from Yokoyama (1996). That advantage of the program can be appreciated when dealing with "thick" piles characterized by large stubbiness ratio r_g / L_p where $r_g = \sqrt{I_p / A_p}$ is the radius of gyration of the pile and L is the pile length. The passage from Timoshenko beam theory to the Euler-Bernoulli is simple in the program: it is effected by setting the shear coefficient equal to zero and by neglecting the rotatory inertial terms (Yokoyama 1996, Przemieniecki 1985).

3.2 Pile model validation under axial vibration

A simple analytical model presented by Holeyman (1992) is used in this section to validate the axial finite element formulation (Fig. 3). The analytical solution models a semi-infinite pile head subjected an impact velocity $V_i = \sqrt{2gH}$ (where g is the gravitational acceleration and H is the impact height) and by a damping constant equal to the pile impedance:

$$I = \rho_p c_p A_p \tag{6}$$

with A_p the pile cross section. The ram has a mass m and the pile head cushion is represented by a spring k allowing both compression and tension.

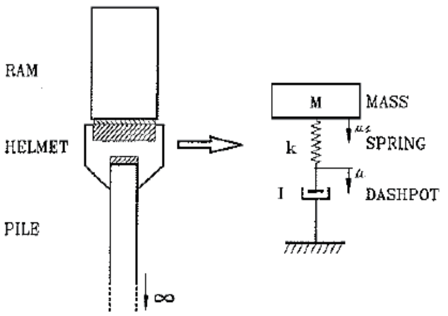

Figure 3. 1-D axial formulation (after Holeyman (1992)).

Figure 4 shows the obtained contours of the maximum velocity ratio $V_{\max} / V_i$ as a function of the cushion stiffness and the ram mass for a given pile impedance of I=1100 kN/ms^{-1}. Thus, maximum force transmitted to the pile is calculated (velocity times impedance) and concrete damaging might be prevented by specifying the maximum strain range $\varepsilon_{\max}$ using the relation:

$$\varepsilon_{\max} = \frac{V_{\max}}{c_p} \tag{7}$$

Figure 5 shows the perfect superposition of the finite element results and the analytical solution for a ram mass equal to 4 tons, a cushion stiffness equal to 2 MN/mm and for values of pile impedance: I=1100 and 2500 kN/ms^{-1}.

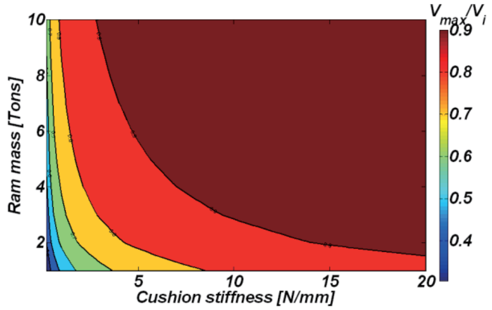

Figure 4. $V_{\max} / V_i$ ($L = \infty$) as function of ram mass and cushion stiffness ratios for H=40 cm and for I=1100 kN/ms^{-1}.

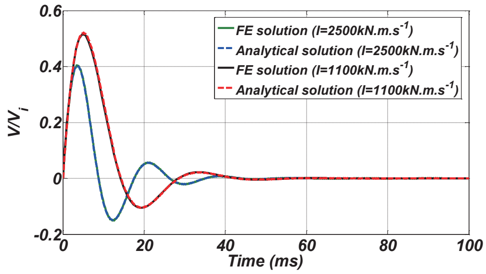

Figure 5. Analytical and finite element solution of a semi-infinite pile.

3.3 Pile model validation under lateral vibration

Before incorporating the soil reaction into the model, it is necessary to validate the numerical results in lateral vibration using available analytical exact solutions. The problem of a simply supported beam was treated as a validation exercise. A modal analysis was performed to calculate the normalized frequencies $f_n = \omega_n \sqrt{\frac{A_p \rho_p L_p^{\ 4}}{E_p I_p}}$ where ω_n is the Eigen circular frequency for mode n.

As shown in Table 1, the normalized calculated frequencies correspond exactly to the analytical ones (Nielsen,1991).

Table1. Calculated normalized frequencies.

Mode	Calculated f_n	Theoretical f_n
1	9.86	9.87
2	39.47	39.48
3	88.82	88.83
4	157.92	157.91
5	246.75	246.74

4 SOIL MODELLING

4.1 *Formulation of Lateral soil vibration*

The dynamic equilibrium conditions within a horizontal plane continuum assuming plane strain conditions can be expressed in terms of the radial and tangential soil displacements (u , v) as follows:

$$\frac{1}{r}\frac{\partial(r\sigma_r)}{\partial r}+\frac{1}{r}\frac{\partial \tau_{r\theta}}{\partial \theta}-\frac{\sigma_\theta}{r}=\rho\frac{\partial^2 u}{\partial t^2} \tag{8}$$

$$\frac{\partial(r^2\tau_{r\theta})}{\partial r}+\frac{1}{r}\frac{\partial \sigma_\theta}{\partial \theta}=\rho\frac{\partial^2 v}{\partial t^2} \tag{9}$$

where r is the radial distance, θ is the circumferential angle, while σ_r , σ_θ and $\tau_{r\theta}$ are the radial, tangential and shear stresses respectively.

These stresses can be related to the displacement field thanks to classical Hooke's relationships based on linear elasticity:

$$\sigma_r=\lambda(\frac{\partial u}{\partial r}+\frac{u}{r}+\frac{1}{r}\frac{\partial v}{\partial \theta})+2G_{r\theta}\frac{\partial u}{\partial r}=\lambda(\varepsilon_r+\varepsilon_\theta)+2G_{r\theta}\varepsilon_r \tag{10}$$

$$\sigma_\theta=\lambda(\frac{\partial u}{\partial r}+\frac{u}{r}+\frac{1}{r}\frac{\partial v}{\partial \theta})+2G_{r\theta}(\frac{u}{r}+\frac{1}{r}\frac{\partial v}{\partial \theta})=\lambda(\varepsilon_r+\varepsilon_\theta)+2G_{r\theta}\varepsilon_\theta \tag{11}$$

$$\tau_{r\theta}=G_{r\theta}(\frac{\partial v}{\partial r}-\frac{v}{r}+\frac{1}{r}\frac{\partial u}{\partial \theta})=G_{r\theta}\gamma_{r\theta} \tag{12}$$

where λ is Lame's first parameter and $G_{r\theta}$ is the lateral shear modulus of the soil.

Figure 6 shows the radial and tangential discretization of the soil continuum within a given horizontal layer. The pile slice of unit thickness is considered rigid in this section.

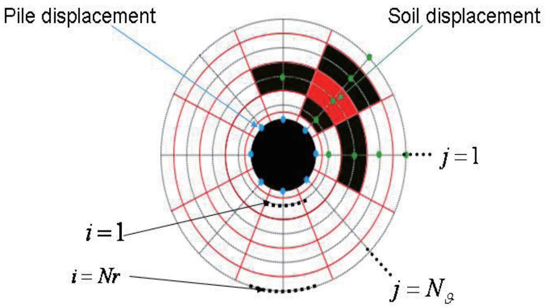

Figure 6. Grid for lateral analysis.

The pile displacement for each circumferential node (blue interface node) must be specified. The soil elements (black elements) are limited according to a 2-D radial grid. The soil hollow slice is discretized according to a number of concentric radial circles N_r (each circle i corresponds to a radial distance r_i) and according to a number of radial lines N_θ representing the circumferential discretization (each line j corresponds an azimuthal angle θ_j).

The grid increments for radial and tangential discretization are respectively Δr and $\Delta\theta$. The mass belonging to each element is lumped at a node (green nodes) where soil acceleration, velocity and displacements are calculated. The mass of each soil element $M(i,j)$ is calculated by $\rho r_i \Delta r \Delta\theta$ where ρ is the soil density.

Strains and stresses have to be calculated between nodes as a result of their relative dispalcement and elastic constants. Using spatial finite differences, strains can be expressed at time step *t*+1 as a function of the soil displacement at time *t* (u^t and v^t):

$$\varepsilon_r^{t+\Delta t}(i,j)=\frac{u^t(i,j)-u^t(i-1,j)}{\Delta r} \tag{13}$$

$$\varepsilon_\theta^{t+\Delta t}(i,j)=\frac{u^t(i,j)}{r_i}+\frac{v^t(i,j)-v^t(i,j-1)}{r_i\Delta\theta} \tag{14}$$

$$\varepsilon_{r\theta}^{t+\Delta t}(i,j)=\frac{v^t(i,j)-v^t(i-1,j)}{\Delta r}-\frac{v^t(i,j)}{r_i}+\frac{u^t(i,j)-u^t(i,j-1)}{r_i\Delta\theta} \tag{15}$$

Once strains are expressed at time *t*+1, stresses are calculated using Equations (10) through (12). Figure 7(a) shows the different stresses around the lumped mass according to the grid discretization. By the projection of theses stresses on the radial r and tangential θ axes for each element (Fig. 7(b)), radial and tangential equilibrium equations are used to compute radial $a_r^{t+\Delta t}(i,j)$ and tangential $a_\theta^{t+\Delta t}(i,j)$ acceleration of soil lumped masses at time t+1.

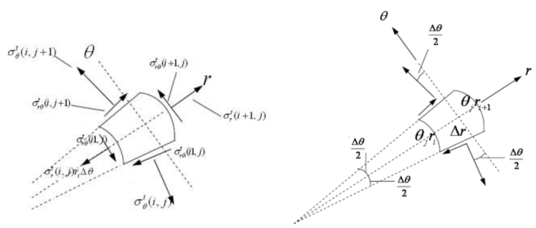

(a) (b)

Figure 7. (a) stresses around soil element
(b) Projection for force calculation

Next, we use the central finite difference time integration (similar to Equations (4) and (5)) to compute soil radial and tangential velocities and displacements at time *t*+1. The latter are reintroduced in Equations (13) to (15) to compute strains for the next time step. The whole numerical process is repeated during the considered time interval.

4.2 Validation of lateral soil vibration

The soil radial discretization model can be validated by imposing a harmonic lateral displacement to a rigid pile disc (Fig. 8). We used for the validation a shear modulus *G*=1 MPa, a Poisson's ratio $\upsilon = 0.4$ and soil density $\rho = 1800\,\text{kg/m}^3$. An imposed displacement with 1 mm amplitude and $\omega = 600\,\text{rad/s}^2$ circular frequency is applied along a direction corresponding to the angle $\theta = 0°$.

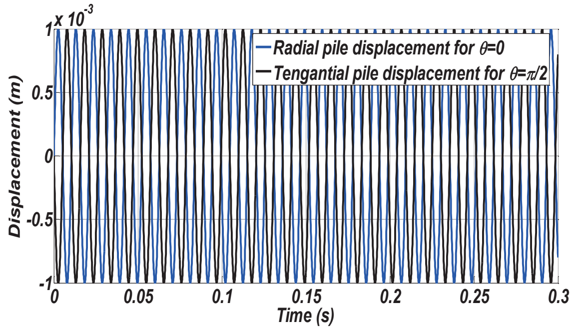

Figure 8. Applied lateral displacement.

The theoretical compressive (P-wave) velocity V_L and shear wave (S-wave) velocity V_s are calculated respectively as:

$$V_s = \sqrt{\frac{G_{r\theta}}{\rho}} = 23{,}5\ \text{m/s} \tag{16}$$

and

$$V_p = \sqrt{\frac{2G_{r\theta}(1-\upsilon)}{\rho(1-2\upsilon)}} = 57{,}7\ \text{m/s} \tag{17}$$

Contours of the radial and tangential displacements are presented in Figures 9 and 10. Close inspection of Figures 9 and 10 demonstrates that calculated P-wave (radial displacement for $\theta = 0°$) and S-wave (tangential displacement for $\theta = \pi/2$) wave propagations correspond exactly to their respective theoretical values.

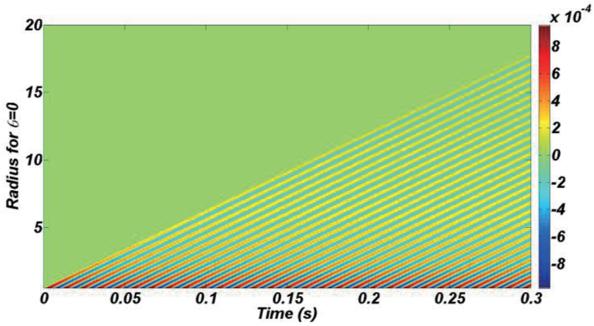

Figure 9. Radial soil displacement [m] along radius $\theta = 0°$.

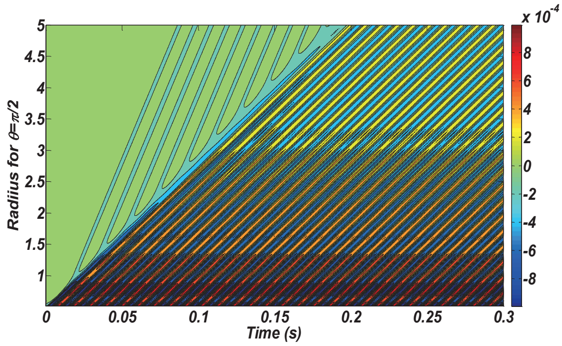

Figure 10. Tangential displacement [m] along $\theta = \pi/2$ radius.

Plane strain steady state solution of Novak's et al (1978) is also compared to the proposed lumped model. Figures 11 and 12 show a great superposition of radial displacement (for $\theta = 0°$) and tangential displacement (for $\theta = \pi/2$), respectively.

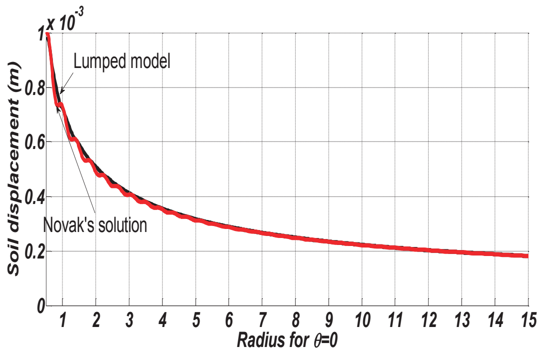

Figure 11. Comparison of analytical and numerical solution for radial displacement along $\theta = 0°$ radius.

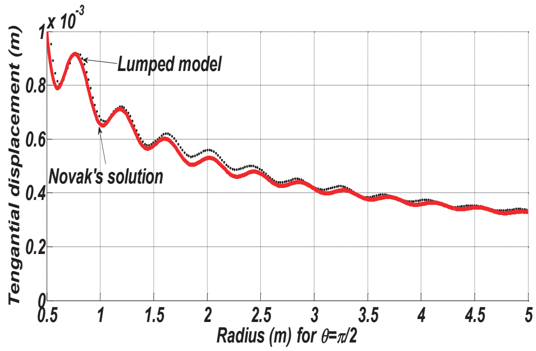

Figure 12: Comparison of analytical and numerical solution for tangential displacement along $\theta = \pi/2$ radius.

5 COUPLED RESULTS OF PILE-SOIL MODELLING

5.1 Coupling between pile and soil models

Once the pile and soil vibration modes are validated, the coupling between pile and soil vibrations is effected through the calculation of the lateral soil resistance at each time step. In fact, the soil lateral resistance is calculated per unit length of pile as:

$$P(r,z,t) = -\int_0^{2\pi} (\sigma_r(r,\theta,t)\cos(\theta) - \tau_{r\theta}(r,\theta,t)\sin(\theta))rd\theta \quad (18)$$

Equation (18) represents the lateral force at a certain radius r, depth z and time t. The lateral resulting force applied on pile is therefore:

$$F_{lat}(z,t) = P(r_0,z,t) \quad (19)$$

The force calculated at the time t from Eq. (19) is further introduced in the pile finite element equation of motion (Eq. (1)) for the time t+1. The same time integration increment is used for both pile and soil models.

5.2 *Comparison with in-situ measurements*

In order to see the practical use of the developed model, a series of eccentric pile dynamic tests were performed. For details on the pile testing experimental program, the reader can refer to Allani and Holeyman (2010, 2012). The pile has approximately a length of 10 m and a 0.35 m side square section. The elastic soil parameters as a function of depth are shows in Table 2.

Table 2. Elastic soil parameter.

Layer N°	$G_{r\theta}$ (MPa)	ν
[0-3] m	58	0.4
[3-7] m	90	0.4
[6-12]	150	0.4

The input loading introduced is the bending moment measured at the pile head with a view to compare simulations to experimental results. Figure 13 shows the measured signals of bending moment for blows n° 4 and 5 along with the drop height H and ram eccentricity e with respect to the pile neutral axis.

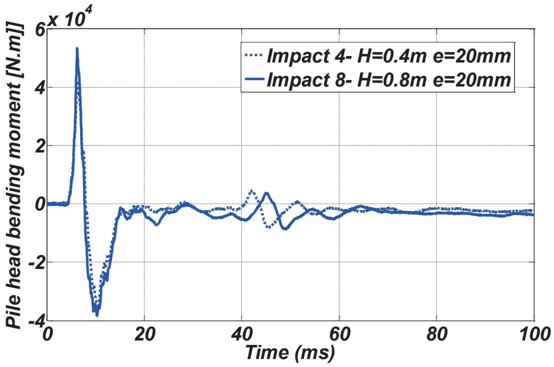

Figure 13. Measured pile head moment.

It was also possible to measure the pile head rotational rates under each impact, thanks to symmetrically placed accelerometers at the pile head. Figures 14 a) and b) show measured and calculated pile head rotation rates for impacts n° 4 and 5. It can be observed that simulations approximate well the measurement at the very beginning of the impact where they are in phase with the measurement and of same order of magnitude.

Although we obtained the same order of magnitude, measured rotation rate is more damped than the calculated one. This is due to the elastic analysis and also to the fact that no additional soil damping is introduced (analogous to Smith damping for axial analysis).

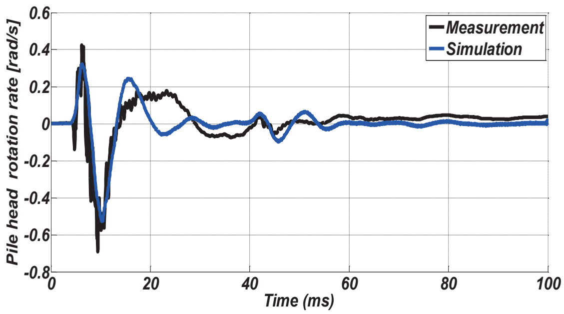

(a)

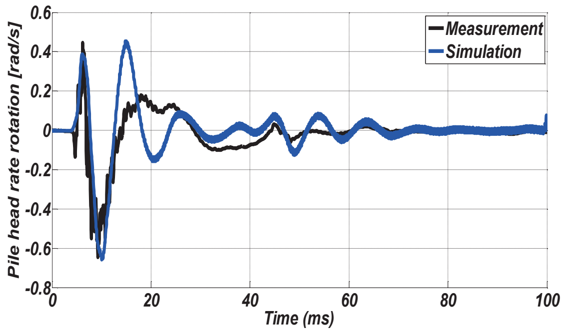

(b)

Figure 14. Comparison of calculated and measured pile head rotation rates.

5.3 *Other important results and other future developments*

The model is also able to estimate the complete pile and soil lateral behavior. For instance, Figures 15 and 16 show respectively the radial and tangential displacement distribution within a 5m deep soil layer at time t=30ms for the problem detailed in Section 5.2.

Maximum values of the calculated lateral pile displacement at the head are on the order of 1 to 2 mm. This value drastically decreases with depth to a value of about 0.01mm at the pile base. The lateral pile and soil displacements are also very important to closely investigate the importance of the eccentricity on the axial pile vibration. In fact, in the authors' opinion transient lateral pile displacement can affect the axial pile bearing capacity estimation. Coupling analyses between axial and lateral vibration modes can significantly improve the post-treatment measured signal in conventional pile driving and pile testing.

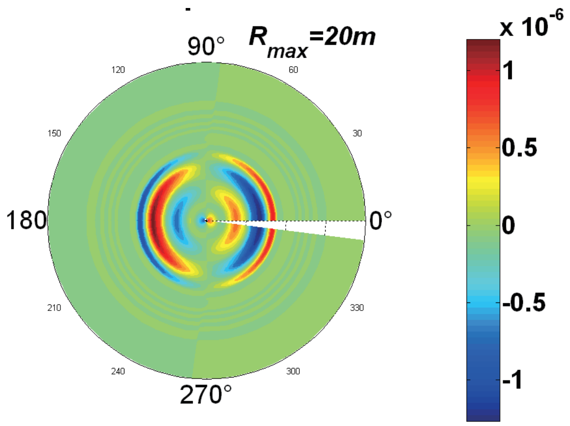

Figure 15.: Radial soil displacement around the pile at depth z=m and at time t=30ms for impact n°4.

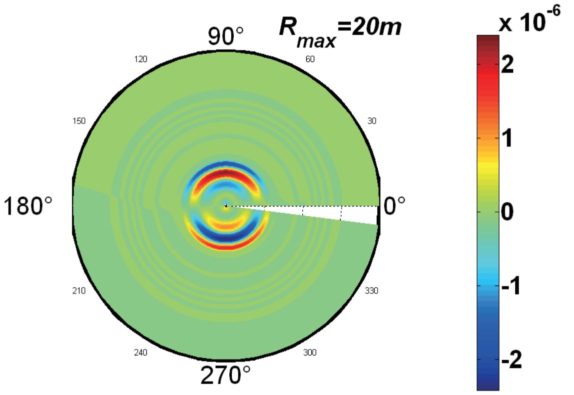

Figure 16. Tangential soil displacement around the pile at depth z=5m and at time t=30ms for impact n°4.

6 CONCLUSION

Lateral pile vibration during pile driving has been addressed by the coupled model suggested in this paper.

The pile is represented by a vertical Euler-Bernoulli beam using finite element method. To properly represent the soil reaction, a continuum approach is used based on lateral 2-D finite difference equations. The pile and the soil reaction are coupled to obtain the whole system response. In the absence of developed numerical programs that estimate and investigate the flexural behavior of the pile in pile driving, the developed numerical program presents a very useful tool step toward that purpose.

Although elastic soil reaction is used herein, the model is versatile and can easily incorporate advanced constitutive law to represent the soil dynamic behavior (Kondner Hyperbolic law (1969), Elastoplastic, Hypoplastic law and so on).

Coupling between axial and lateral pile vibration modes can be effected thanks to the developed programs. This will allow the determination of the flexural effects on the axial measurement and pile bearing capacity.

The Timoshenko beam theory is also implemented in the finite element pile formulation. This feature can be helpful for thick beams. Furthermore the benefits of eccentric impact could be explored more closely by using the Timoshenko beam theory to investigate the developed shear forces between the pile, cushion and mass (Allani and Holeyman 2010).

REFERENCES

Abramson H.N (1957). Flexural waves in elastic beams of circular cross section. The journal of Acoustical society of America V29, N°1, 42-46.

Achenbach J.D (1980). Wave propagation in elastic solids. North Holland .

Allani. M and Holeyman A. (2010). Non axial effects in dynamic pile testing: Pile vibration analysis using Timoshenko beam theory. Geotechnical Engineering 20, View of Young European Geotechnical Engineers, Brno, 158-163.

Allani M and Holeyman A (2010). Signal analysis of axial and flexural behavior in high strain dynamic pile testing. Proceedings of the 2nd International conference on Geotechnical Engineering, Hammamet, Tunisia, 477-486.

Allani M and Holeyman A (2012). Flexural behavior of pile in high strain dynamic pile testing. Submitted to the 9th International Conference on testing and Design Methods for Deep Foundation. IS-Kanazawa. Japan.

Charue N (2004), Loading rate effects on pile load-displacement behavior derived from back calculation analysis of two load testing procedure.

Chau KT, Yang X. (2005). Nonlinear interaction of soil-pile in horizontal vibration. Journal of Engineering Mechanics ACSE. 847:858-131(8).

El Naggar M. H, Novak M. (1995). Nonlinear lateral interaction in pile dynamics, Soil dynamics and earthquake engineering; 141:157-14.

El Naggar MH, Novak M. (1996).Nonlinear analysis for dynamic lateral pile response. Soil dynamics and earthquake engineering. 223:244-15(4).

Goble G G. (2000). Keynote lecture: some wave mechanics applications. Application of Stress waves theory to piles.

Holeyman A. E. (1984). Contribution à l'étude du comportement transitoire non-lineaire des pieux pendant leur battage. Thesis dissertation. Université Libre de Bruxelles (ULB), 584p.

Holeyman A. E. (1992). Keynote lecture: Technology of pile dynamics. Proceedings of the fourth international conference on the application of stress wave theory to piles. 195-215. A.A Balkema, Rotterdam, Netherlands.

Holeyman. A, Legrand. C (1994). Soil modeling for pile vibratory driving. International Conference on Design and Construction of Deep Foundation, Orlando. 1165-1178(2).

Holeyman A.E (2000), Keynote lecture: Technology of Pile dynamics, Application of Stress waves theory to piles, 195-215.
Ishihara K. (1996). Soil behaviour in earthquake geotechnics. Oxford Clarendon Press;
Kondner R.L (1963), Hyperbolic stress strain response: cohesive soils. Journal of soil Mechanics and Foundations Division. 115:143-89.
Nielsen J.C.O (1991). Eigenfrequencies and eigenmodes for beam structures on an elastic foundation. Journal of sound and vibration; 145(3): 479-487.
Nogami T, Novak M. (1977). Resistance of soil to a horizontally vibrating pile. Earthquake Engineering and Structural Dynamics. 249:261-5.
Novak M, Nogami T, Aboul-ella F. (1978). Dynamic soil reactions for plane strain case. Journal of Mechanical Engineering Div ASCE; 953:959-104
Novak M. (1977). Vertical vibration of floating piles. Journal of Engineering Mechanics Division; 153:168-103(1).
Novak M. (1974). Dynamic Stiffness and Damping of Piles. Canadian Geotechnical Journal, 574:598-11(4)
Novak. M and Sheta. (1980). M. Approximate approach to contact effects of piles. Proc of Dynamic response of pile found: Analytical aspects ASCE . New York, N.Y 53-79.
Novak M, Nogami T. (1977). Soil-pile interaction in horizontal vibration. Earthquake Engineering and Structural Dynamics; 263:281-5.
Poskitt T.J. (1991). Energy loses in pile driving due to soil rate effects and hammer misalignment. Proceedings Institution of Civil Engineers; 823:851-91.
Poskitt T.J. (1992). Keynote lecture: problems of reconciling stress wave measurements with theory. Proceedings of the fourth international conference on the application of stress wave theory to piles, 495-507. A.A BALKEMA, Rotterdam, Netherlands.
Poskitt T.J. (1996). The deflection of piles during driving. Géotechnique, 46 (2), 235 –243
Rausche F, Goble G.G, Likins G.E. (1985) Dynamic determination of pile capacity, Journal of geotechnical Engineering, 11, 367-383.
Przemieniecki J.S.(1985). Theory of matrix structural theory. Dover Publications.
Rauche F. (2000). Keynote lecture: pile driving equipment: Capabilities and properties Application of Stress waves theory to piles.
Smith, E.A.L. (1960). Pile driving analysis by the wave Equation. Journal of soil mechanics and foundation division.(ASCE). 6(4), 35-61.
Yao S and Nogami T (1994). Lateral cyclic response on pile in viscoelastic Winkler subgrade. Journal of engeneering mechanics 120, 758-775.
Yokoyama T (1996), vibration analysis of Timoshenko beam-column on two-parameter elastic foundation, Computers and Structure 995-107.
VanAlboom G, and Whenham V. (2003). Soil investigation campaign at Limelette (Belgium) Results. In Proceeding of the Symposium on screw piles in sand. Design and recent development Swts and Zeitlinger, Eds.